ANL-HEP-PR-99-97

JLAB-THY-99-27

Spin Dependence of Massive Lepton Pair Production in Proton-Proton Collisions

Edmond L. Berger[a], Lionel E. Gordon[b,c], and Michael Klasen[a]

[a] *High Energy Physics Division, Argonne National Laboratory*

Argonne, Illinois 60439

[b] *Jefferson Laboratory, Newport News, VA 23606*

[c] *Hampton University, Hampton, VA 23668*

(September 20, 1999)

Abstract

We calculate the transverse momentum distribution for the production of massive lepton-pairs in longitudinally polarized proton-proton reactions at collider energies within the context of perturbative quantum chromodynamics. For values of the transverse momentum Q_T greater than roughly half the pair mass Q, $Q_T > Q/2$, we show that the differential cross section is dominated by subprocesses initiated by incident gluons, provided that the polarized gluon density is not too small. Massive lepton-pair differential cross sections should be a good source of independent constraints on the polarized gluon density, free from the experimental and theoretical complications of photon isolation that beset studies of prompt photon production. We provide predictions for the spin-averaged and spin-dependent differential cross sections as a function of Q_T at energies relevant for the Relativistic Heavy Ion Collider (RHIC) at Brookhaven, and we compare these with predictions for real prompt photon

production.

12.38.Bx, 12.38.Qk, 13.85.Qk, 13.88.+e

Typeset using REVTEX

I. INTRODUCTION AND MOTIVATION

Both massive lepton-pair production, $h_1 + h_2 \to \gamma^* + X; \gamma^* \to l\bar{l}$, and prompt real photon production, $h_1 + h_2 \to \gamma + X$ are valuable probes of short-distance behavior in hadron reactions. The two reactions supply critical information on parton momentum densities, in addition to the opportunities they offer for tests of perturbative quantum chromodynamics (QCD). Spin-averaged parton momentum densities may be extracted from spin-averaged nucleon-nucleon reactions, and spin-dependent parton momentum densities from spin-dependent nucleon-nucleon reactions. An ambitious experimental program of measurements of spin-dependence in polarized proton-proton reactions will begin soon at Brookhaven's Relativistic Heavy Ion Collider (RHIC) with kinematic coverage extending well into the regions of phase space in which perturbative quantum chromodynamics should yield reliable predictions.

Massive lepton-pair production, commonly referred to as the Drell-Yan process [1], provided early confirmation of three colors and of the size of next-to-leading contributions to the cross section differential in the pair mass Q. The mass and longitudinal momentum (or rapidity) dependences of the cross section (integrated over the transverse momentum Q_T of the pair) serve as laboratory for measurement of the *antiquark* momentum density, complementary to deep-inelastic lepton scattering from which one gains information of the sum of the quark and antiquark densities. Inclusive prompt real photon production is a source of essential information on the *gluon* momentum density. At lowest order in perturbation theory, the reaction is dominated at large values of the transverse momentum p_T of the produced photon by the "Compton" subprocess, $q + g \to \gamma + q$. This dominance is preserved at higher orders, indicating that the experimental inclusive cross section differential in p_T may be used to determine the density of gluons in the initial hadrons [2–5].

In two previous papers [6], we addressed the production of massive lepton-pairs as a function of the transverse momentum Q_T of the pair in unpolarized nucleon-nucleon reactions, $h_1 + h_2 \to \gamma^* + X$, in the region where Q_T is greater than roughly half of the mass of the

pair, $Q_T > Q/2$. We demonstrated that the differential cross section in this region is dominated by subprocesses initiated by incident gluons. Correspondingly, massive lepton-pair differential cross sections in unpolarized nucleon-nucleon reactions are a valuable, heretofore overlooked, independent source of constraints on the spin-averaged gluon density.

Turning to longitudinally polarized proton-proton collisions in this paper, we study the potential advantages that the Drell-Yan process may offer for the determination of the spin-dependence of the gluon density. To be sure, the cross section for massive lepton-pair production is smaller than it is for prompt photon production. However, just as in the unpolarized case, massive lepton pair production is cleaner theoretically since long-range fragmentation contributions are absent as are the experimental and theoretical complications associated with isolation of the real photon. Moreover, the dynamics of spin-dependence in hard-scattering processes is a sufficiently complex topic, and its understanding at an early stage in its development, that several defensible approaches for extracting polarized parton densities deserve to be pursued with the expectation that consistent results must emerge.

There are notable similarities and differences in the theoretical analyses of massive lepton-pair production and prompt real photon production. At first-order in the strong coupling strength, α_s, the Compton subprocess and the annihilation subprocess $q + \bar{q} \to \gamma + g$ supply the transverse momentum of the *directly* produced prompt photons. Identical subprocesses, with the real γ replaced by a virtual γ^*, are responsible at $\mathcal{O}(\alpha_s)$ for the transverse momentum of massive lepton-pairs. An important distinction, however, is that fragmentation subprocesses play a very important role in prompt real photon production at collider energies. In these long-distance fragmentation subprocesses, the photon emerges from the fragmentation of a final parton, e.g., $q + g \to q + g$, followed by $q \to \gamma + X$. The necessity to invoke phenomenological fragmentation functions and the infrared ambiguity [7] of the isolated cross section in next-to-leading order raise questions about the extent to which isolated prompt photon data may be used for fully quantitative determinations of the gluon density. It is desirable to investigate other physical processes for extraction of the gluon density that are free from these systematic uncertainties. Fortunately, no isolation would

seem necessary in the case of virtual photon production (and subsequent decay into a pair of muons) in typical collider or fixed target experiments. Muons are observed only after they have penetrated a substantial hadron absorber. Thus, any hadrons within a typical cone about the direction of the γ^* will have been stopped, and the massive lepton-pair signal will be entirely inclusive.

Another significant distinction between massive lepton-pair production and prompt real photon production is that interest in $h_1 + h_2 \to \gamma^* + X$ has been drawn most often to the domain in which the pair mass Q is relatively large, justifying a perturbative treatment based on a small value of $\alpha_s(Q)$ and the neglect of inverse-power high-twist contributions (except near the edges of phase space). The focus in prompt real photon production is directed to the region of large values of p_T where $\alpha_s(p_T)$ is small. Interest in the transverse momentum Q_T dependence of the massive lepton-pair production cross section has tended to be limited to small values of Q_T where the cross section is largest. Fixed-order perturbation theory [8] is applicable for large Q_T, but it is inadequate at small Q_T, and all-orders resummation methods [9–13] have been developed to address the region $Q_T << Q$.

As long as Q_T is large, the perturbative requirement of small $\alpha_s(Q_T)$ can be satisfied without a large value of Q. We therefore explore and advocate the potential advantages of studies of $d^2\sigma/dQdQ_T$ as a function of Q_T for modest values of Q, $Q \sim 2$ to 3 GeV, below the range of the traditional Drell-Yan region. There are various backgrounds with which to contend at small Q such as the contributions to the event rate from prompt decays of heavy flavors, e.g., $h_1 + h_2 \to c + \bar{c} + X; c \to l + X$. These heavy flavor contributions may be estimated by direct computation [14] and/or bounded through experimental measurement of the like-sign-lepton distributions.

In Sec. II, we review perturbative QCD calculations of the transverse momentum distribution for massive lepton-pair production in the case in which the initial nucleon spins are polarized as well as in the spin-average case. In Sec. III, we present next-to-leading order predictions for the transverse momentum dependence of the cross sections for massive lepton-pair and real prompt photon production in unpolarized proton-proton collisions

at energies typical of the RHIC collider. Predictions for spin dependence are provided in Sec. IV. Our conclusions are summarized in Sec. V.

II. MASSIVE LEPTON PAIR PRODUCTION AND PROMPT PHOTON PRODUCTION AT NEXT-TO-LEADING ORDER

In inclusive hadron interactions at collider energies, $h_1+h_2 \to \gamma^*+X$ with $\gamma^* \to l\bar{l}$, lepton pair production proceeds through partonic hard-scattering processes involving initial-state light quarks q and gluons g. In lowest-order QCD, at $\mathcal{O}(\alpha_s^0)$, the only partonic subprocess is $q+\bar{q} \to \gamma^*$. At $\mathcal{O}(\alpha_s)$, both $q+\bar{q} \to \gamma^*+g$ and $q+g \to \gamma^*+q$ participate, with the recoil of the final parton balancing the transverse momentum of the lepton-pair. These processes are shown in Figs. 1(a) and 2(a). Calculations of the cross section at order $\mathcal{O}(\alpha_s^2)$ involve virtual loop corrections to these $\mathcal{O}(\alpha_s)$ subprocesses (Figs. 1(b) and 2(b)) as well as contributions from a wide range of $2 \to 3$ parton subprocesses (of which some examples are shown in Figs. 1(c) and 2(c)).

The physical cross section is obtained through the factorization theorem,

$$\frac{d^2\sigma^{\gamma^*}_{h_1h_2}}{dQ_T^2 dy} = \sum_{ij} \int dx_1 dx_2 f^i_{h_1}(x_1,\mu_f^2) f^j_{h_2}(x_2,\mu_f^2) \frac{s d^2\hat{\sigma}^{\gamma^*}_{ij}}{dtdu}(s,Q,Q_T,y;\mu_f^2). \tag{1}$$

It depends on the hadronic center-of-mass energy S and on the mass Q, the transverse momentum Q_T, and the rapidity y of the virtual photon; μ_f is the factorization scale of the scattering process. The usual Mandelstam invariants in the partonic system are defined by $s=(p_1+p_2)^2$, $t=(p_1-p_{\gamma^*})^2$, and $u=(p_2-p_{\gamma^*})^2$, where p_1 and p_2 are the momenta of the initial state partons and p_{γ^*} is the momentum of the virtual photon. The indices $ij \in \{q\bar{q}, qg\}$ denote the initial parton channels whose contributions are added incoherently to yield the total physical cross section. Functions $f^j_h(x,\mu)$ denote the usual spin-averaged parton distribution functions.

The partonic cross section $\hat{\sigma}^{\gamma^*}_{ij}(s,Q,Q_T,y;\mu_f^2)$ is obtained commonly from fixed-order QCD calculations through

$$\frac{d^2\hat{\sigma}_{ij}^{\gamma^*}}{dtdu} = \alpha_s(\mu^2)\frac{d^2\hat{\sigma}_{ij}^{\gamma^*,(a)}}{dtdu} + \alpha_s^2(\mu^2)\frac{d^2\hat{\sigma}_{ij}^{\gamma^*,(b)}}{dtdu} + \alpha_s^2(\mu^2)\frac{d^2\hat{\sigma}_{ij}^{\gamma^*,(c)}}{dtdu} + \mathcal{O}(\alpha_s^3). \tag{2}$$

The tree, virtual loop, and real emission contributions are labeled (a), (b), and (c) as are the corresponding diagrams in Figs. 1 and 2. The parameter μ is the renormalization scale. It is set equal to the factorization scale $\mu_f = \sqrt{Q^2 + Q_T^2}$ throughout this paper.

The cross section for $h_1 + h_2 \to l\bar{l} + X$, differential in the invariant mass of the lepton pair Q^2 as well as its transverse momentum and rapidity, is obtained from Eq. (1) by the relation

$$\frac{d^3\sigma_{h_1h_2}^{l\bar{l}}}{dQ^2dQ_T^2dy} = \left(\frac{\alpha_{em}}{3\pi Q^2}\right)\frac{d^2\sigma_{h_1h_2}^{\gamma^*}}{dQ_T^2dy}(S, Q, Q_T, y), \tag{3}$$

where $Q^2 = (p_l + p_{\bar{l}})^2$, and $p_l, p_{\bar{l}}$ are the four-momenta of the two final leptons. The Drell-Yan factor $\alpha_{em}/(3\pi Q^2)$ is included in all numerical results presented in this paper.

While the full next-to-leading order QCD calculation exists for massive lepton-pair production in the case of unpolarized initial nucleons, only a partial calculation is available in the polarized case [15]. Correspondingly, we present spin-averaged differential cross sections at next-to-leading order, but we calculate spin asymmetries at leading order. Spin asymmetries are obtained by dividing the spin-dependent differential cross section by its spin-averaged counterpart. For prompt photon production, comparisons of asymmetries computed at next-to-leading order with those at leading order show only modest differences [16], whereas the cross sections themselves are affected more significantly. Given the similarity of prompt photon production and massive lepton-pair production in the region of Q_T of interest to us [6], we expect that the leading-order asymmetries will serve as a useful guide for massive lepton-pair production.

Rewriting Eq. (3) and integrating over an interval in Q^2, we calculate the spin-averaged differential cross section $Ed^3\sigma_{h_1h_2}^{l\bar{l}}/dp^3$ as

$$\frac{Ed^3\sigma_{h_1h_2}^{l\bar{l}}}{dp^3} = \frac{\alpha_{em}}{3\pi^2 S}\sum_{ij}\int_{Q^2_{min}}^{Q^2_{max}}\frac{dQ^2}{Q^2}\int_{x_1^{min}}^1\frac{dx_1}{x_1 - \bar{x}_1}f_{h_1}^i(x_1, \mu_f^2)f_{h_2}^j(x_2, \mu_f^2)s\frac{d\hat{\sigma}_{ij}^{\gamma^*}}{dt}. \tag{4}$$

In Eq. (4), Q^2_{max} and Q^2_{min} are the chosen upper and lower limits of integration for Q^2, and

$x_1^{min} = (\bar{x}_1 - \tau)/(1 - \bar{x}_2)$. The value of x_2 is determined from $x_2 = (x_1\bar{x}_2 - \tau)/(x_1 - \bar{x}_1)$, with

$$\bar{x}_1 = \frac{Q^2 - U}{S} = \frac{1}{2}e^y\sqrt{x_T^2 + 4\tau}, \tag{5}$$

and

$$\bar{x}_2 = \frac{Q^2 - T}{S} = \frac{1}{2}e^{-y}\sqrt{x_T^2 + 4\tau}. \tag{6}$$

We use P_1 and P_2 to denote the four-vector momenta of the incident nucleons; $S = (P_1+P_2)^2$. The invariants in the hadronic system, $T = (P_1 - p_{\gamma^*})^2$ and $U = (P_2 - p_{\gamma^*})^2$, are related to the partonic invariants by

$$(t - Q^2) = x_1(T - Q^2) = -x_1\bar{x}_2 S, \tag{7}$$

and

$$(u - Q^2) = x_2(U - Q^2) = -x_2\bar{x}_1 S. \tag{8}$$

The scaled variables x_T and τ are

$$x_T = \frac{2Q_T}{\sqrt{S}}, \quad \tau = \frac{Q^2}{S}.$$

When the initial nucleons are polarized longitudinally, we can compute the difference of cross sections

$$\Delta\sigma = \sigma_{++} - \sigma_{+-}, \tag{9}$$

where $+, -$ denote the helicities of the incident nucleons.

In analogy to Eq. (4), we find

$$\frac{Ed^3\Delta\sigma^{l\bar{l}}_{h_1h_2}}{dp^3} = \frac{\alpha_{em}}{3\pi^2 S}\sum_{ij}\int_{Q^2_{min}}^{Q^2_{max}}\frac{dQ^2}{Q^2}\int_{x_1^{min}}^1 \frac{dx_1}{x_1 - \bar{x}_1}\Delta f^i_{h_1}(x_1,\mu_f^2)\Delta f^j_{h_2}(x_2,\mu_f^2)s\frac{d\Delta\hat{\sigma}^{\gamma^*}_{ij}}{dt}. \tag{10}$$

The functions $\Delta f^j_h(x,\mu)$ denote the spin-dependent parton distribution functions, defined by

$$\Delta f_h^i(x,\mu_f) = f_{h,+}^i(x,\mu_f) - f_{h,-}^i(x,\mu_f); \tag{11}$$

$f_{h\pm}^i(x,\mu_f)$ is the distribution of partons of type i with positive $(+)$ or negative $(-)$ helicity in hadron h. Likewise, the polarized partonic cross section $\Delta\hat{\sigma}^{\gamma^*}$ is defined by

$$\Delta\hat{\sigma}^{\gamma^*} = \hat{\sigma}^{\gamma^*}(+,+) - \hat{\sigma}^{\gamma^*}(+,-), \tag{12}$$

with $+,-$ denoting the helicities of the incoming partons.

The hard subprocess cross sections in leading order for the unpolarized and polarized cases are

$$s\frac{d\hat{\sigma}_{q\bar{q}}}{dt} = -s\frac{d\Delta\hat{\sigma}_{q\bar{q}}}{dt} = e_q^2\frac{2\pi\alpha_{em}C_F}{N_C}\frac{\alpha_s}{s}\left[\frac{u}{t}+\frac{t}{u}+\frac{2Q^2(Q^2-u-t)}{ut}\right], \tag{13}$$

$$s\frac{d\sigma_{qg}}{dt} = -e_q^2\frac{\pi\alpha_{em}}{N_C}\frac{\alpha_s}{s}\left[\frac{s}{t}+\frac{t}{s}+\frac{2Q^2u}{st}\right], \tag{14}$$

and

$$s\frac{d\Delta\sigma_{qg}}{dt} = e_q^2\frac{\pi\alpha_{em}}{N_C}\frac{\alpha_s}{s}\left[\frac{2u+s}{t}-\frac{2u+t}{s}\right]. \tag{15}$$

Our results on the longitudinal spin dependence are expressed in terms of the two-spin longitudinal asymmetry A_{LL}, defined by

$$A_{LL} = \frac{\sigma^{\gamma^*}(+,+)-\sigma^{\gamma^*}(+,-)}{\sigma^{\gamma^*}(+,+)+\sigma^{\gamma^*}(+,-)}, \tag{16}$$

where $+,-$ denote the helicities of the incoming protons.

III. UNPOLARIZED CROSS SECTIONS

We turn in this Section to explicit evaluations of the differential cross sections as functions of Q_T at collider energies. We work in the $\overline{\rm MS}$ renormalization scheme and set the renormalization and factorization scales equal. We employ the MRST set of spin-averaged parton densities [17] and a two-loop expression for the strong coupling strength $\alpha_s(\mu)$, with five flavors and appropriate threshold behavior at $\mu = m_b$; $\Lambda^{(4)} = 300$ MeV. The strong

coupling strength α_s is evaluated at a hard scale $\mu = \sqrt{Q^2 + Q_T^2}$. We present results for three values of the center-of-mass energy, $\sqrt{S} = 50$, 200, and 500 GeV.

For $\sqrt{S} = 200$ GeV, we present the invariant inclusive cross section $Ed^3\sigma/dp^3$ as a function of Q_T in Fig. 3. Shown in this figure are the $q\bar{q}$ and qg perturbative contributions to the cross section at leading order and at next-to-leading order. We average the invariant inclusive cross section over the rapidity range -1.0 $< y <$ 1.0 and over the mass interval 5 $< Q <$ 6 GeV. For $Q_T <$ 1.5 GeV, the $q\bar{q}$ contribution exceeds that of qg channel. However, for values of $Q_T >$ 1.5 GeV, the qg contribution becomes increasingly important. As shown in Fig. 4(a), the qg contribution accounts for about 80 % of the rate once $Q_T \simeq Q$. The results in Fig. 4(a) also demonstrate that subprocesses other than those initiated by the $q\bar{q}$ and qg initial channels contribute negligibly.

In Fig. 4(b), we display the fractional contributions to the cross section as a function of Q_T for a larger value of Q: 11 $< Q <$ 12 GeV. In this case, the fraction of the rate attributable to qg initiated subprocesses again increases with Q_T. It becomes 80 % for $Q_T \simeq Q$.

For the calculations reported in Figs. 3 and 4(a,b), we chose values of Q in the traditional range for studies of massive lepton-pair production, viz., above the interval of the J/ψ and ψ' states and either below or above the interval of the $\Upsilon's$.

For Fig. 4(c), we select the interval 2.0 $< Q <$ 3.0 GeV. In this region, one would be inclined to doubt the reliability of leading-twist perturbative descriptions of the cross section $d\sigma/dQ$, *integrated* over all Q_T. However for values of Q_T that are large enough, a perturbative description of the Q_T dependence of $d^2\sigma/dQdQ_T$ ought to be justified. The results presented in Fig. 4(c) demonstrate that, as at higher masses, the qg incident subprocesses dominate the cross section for $Q_T \simeq Q$.

The calculations presented in Figs. 4 show convincingly that data on the transverse momentum dependence of the cross section for massive lepton-pair production at RHIC collider energies should be a valuable independent source of information on the spin-averaged

gluon density.

In Fig. 5, we provide next-to-leading order predictions of the differential cross section as a function of Q_T for three values of the center-of-mass energy and two intervals of mass Q. Taking $Ed^3\sigma/dp^3 = 10^{-3}\text{pb/GeV}^2$ as the minimum accessible cross section, we may use the curves in Fig. 5 to establish that the massive lepton-pair cross section may be measured to $Q_T = 7.5$, 14, and 18.5 GeV at $\sqrt{S} = 50$, 200, and 500 GeV, respectively, when $2 < Q < 3$ GeV, and to $Q_T = 6$, 11.5, and 15 GeV when $5 < Q < 6$ GeV. In terms of reach in the fractional momentum x_{gluon} carried by the gluon, these values of Q_T may be converted to $x_{gluon} \simeq x_T = 2Q_T/\sqrt{S} = 0.3$, 0.14, and 0.075 at $\sqrt{S} = 50$, 200, and 500 GeV when $2 < Q < 3$ GeV, and to $x_{gluon} \simeq 0.24$, 0.115, and 0.06 when $5 < Q < 6$ GeV. On the face of it, the smallest value of $\sqrt{S}$ provides the greatest reach in x_{gluon}. However, the reliability of fixed-order perturbative QCD as well as dominance of the qg subprocess improve with greater Q_T. The maximum value $Q_T \simeq 7.5$ GeV attainable at $\sqrt{S} = 50$ GeV argues for a larger $\sqrt{S}$.

It is instructive to compare our results with those expected for prompt real photon production. In Fig. 6, we present the predicted differential cross section for prompt photon production for three center-of-mass energies. We display the result with full fragmentation taken into consideration (upper line) and with no fragmentation contributions included (lower line). Comparing the magnitudes of the prompt photon and massive lepton pair production cross sections in Figs. 5 and 6, we note that the inclusive prompt photon cross section is a factor of 1000 to 4000 greater than the massive lepton-pair cross section integrated over the mass interval $2.0 < Q < 3.0$ GeV, depending on the value of Q_T. This factor is attributable in large measure to the factor $\alpha_{em}/(3\pi Q^2)$ associated with the decay of the virtual photon to $\mu^+\mu^-$. Again taking $Ed^3\sigma/dp^3 = 10^{-3}\text{pb/GeV}^2$ as the minimum accessible cross section, we may use the curves in Fig. 6 to establish that the real photon cross section may be measured to $p_T = 14$, 33, and 52 GeV at $\sqrt{S} = 50$, 200, and 500 GeV, respectively. The corresponding reach in $x_T = 2p_T/\sqrt{S} = 0.56$, 0.33, and 0.21 at $\sqrt{S} = 50$, 200, and 500 GeV is two to three times that of the massive lepton-pair case.

The breakdown of the real photon direct cross section at $\sqrt{S} = 200$ GeV into its $q\bar{q}$ and qg components is presented in Fig. 7. As may be appreciated from a comparison of Figs. 4 and 7, dominance of the qg contribution in the massive lepton-pair case is as strong as in the prompt photon case. The significantly smaller cross section in the case of massive lepton-pair production means that the reach in x_{gluon} is restricted to about a factor of two to three less, depending on $\sqrt{S}$ and Q, than that potentially accessible with prompt photons in the same sample of data. Nevertheless, it is valuable to be able to investigate the gluon density with a process that has reduced experimental and theoretical systematic uncertainties from those of the prompt photon case.

In our previous papers [6] we compared our spin-averaged cross sections with available fixed-target and collider data on massive lepton-pair production at large values of Q_T, and we were able to establish that fixed-order perturbative calculations, without resummation, should be reliable for $Q_T > Q/2$. The region of small Q_T and the matching region of intermediate Q_T are complicated by some level of phenomenological ambiguity. Within the resummation approach, phenomenological non-perturbative functions play a key role in fixing the shape of the Q_T spectrum at very small Q_T, and matching methods in the intermediate region are hardly unique. For the goals we have in mind, it would appear best to restrict attention to the region $Q_T \geq Q/2$.

IV. PREDICTIONS FOR SPIN DEPENDENCE

Given theoretical expressions derived in Sec. II that relate the spin-dependent cross section at the hadron level to spin-dependent partonic hard-scattering matrix elements and polarized parton densities, we must adopt models for spin-dependent parton densities in order to obtain illustrative numerical expectations. For the spin-dependent densities that we need, we use the three different parametrizations suggested by Gehrmann and Stirling (GS) [18]. We have verified that the positivity requirement $\left|\Delta f_h^j(x,\mu_f)/f_h^j(x,\mu_f)\right| \leq 1$ is satisfied.

The current deep inelastic scattering data do not constrain the polarized gluon density tightly, and most groups present more than one plausible parametrization. Gehrmann and Stirling [18] present three such parametrizations, labelled GSA, GSB, and GSC. In the GSA and GSB sets, $\Delta G(x, \mu_o)$ is positive for all x, whereas in the GSC set $\Delta G(x, \mu_o)$ changes sign. After evolution to $\mu_f^2 = 100$ GeV^2, $\Delta G(x, \mu_f)$ remains positive for essentially all x in all three sets, but its magnitude is small in the GSB and GSC sets.

In this Section, we present two-spin longitudinal asymmetries for massive lepton-pair production as a function of transverse momentum. Results are displayed for pp collisions at the center-of-mass energies $\sqrt{S} = 50$, 200, and 500 GeV typical of the Brookhaven RHIC collider.

In Figs. 8(a-c), we present the two-spin longitudinal asymmetries, A_{LL}, as a function of Q_T. As noted earlier, these asymmetries are computed in leading-order. More specifically, we use leading-order partonic subprocess cross sections $\hat{\sigma}$ and $\Delta\hat{\sigma}$ with next-to-leading order spin-averaged and spin-dependent parton densities and a two-loop expression for α_s. The choice of a leading-order expression for $\Delta\hat{\sigma}$ is required because the full next-to-leading order derivation of $\Delta\hat{\sigma}$ has not been completed for massive lepton-pair production. Experience with prompt photon production indicates that the leading-order and next-to-leading order results for the asymmetry are similar so long as both are dominated by the qg subprocess. Results are shown for three choices of the polarized gluon density. The asymmetry becomes sizable for large enough Q_T for the GSA and GSB parton sets but not in the GSC case. Comparing the three figures, we note that A_{LL} is nearly independent of the pair mass Q as long as Q_T is not too small. This feature should be helpful for the accumulation of statistics; small bin-widths in mass are not necessary, but the J/ψ and Υ resonance regions should be excluded.

As noted above the qg subprocess dominates the *spin-averaged* cross section. It is interesting and important to inquire whether this dominance persists in the spin-dependent situation. In Figs. 9 and 10, we compare the contribution to the asymmetry from the polarized qg subprocess with the complete answer for all three sets of parton densities. The qg

contribution is more positive than the full answer for values of Q_T that are not too small; the full answer is reduced by the negative contribution from the $q\bar{q}$ subprocess for which the parton-level asymmetry $\hat{a}_{LL} = -1$. At small Q_T, the net asymmetry may be driven negative by the $q\bar{q}$ contribution, and based on our experience with other calculations [19], from processes such as gg that contribute in next-to-leading order. For the GSA and GSB sets, we see that once it becomes sizable (e.g., 5% or more), the total asymmetry from all subprocesses is dominated by the large contribution from the qg subprocess.

As a general rule in studies of polarization phenomena, many subprocesses can contribute small and conflicting asymmetries. Asymmetries are readily interpretable only in situations where the basic dynamics is dominated by one major subprocess and the overall asymmetry is sufficiently large. In the case of massive lepton-pair production that is the topic of this paper, when the overall asymmetry A_{LL} itself is small, the contribution from the qg subprocess cannot be said to dominate the answer. However, if a large asymmetry is measured, similar to that expected in the GSA case at the larger values of Q_T, Figs. 9 and 10 show that the answer is dominated by the qg contribution, and data will serve to constrain $\Delta G(x, \mu_f)$. If $\Delta G(x, \mu_f)$ is small and a small asymmetry is measured, such as for the GSC parton set, or at small Q_T for all parton sets, one will not be able to conclude which of the subprocesses is principally responsible, and no information could be adduced about $\Delta G(x, \mu_f)$, except that it is small.

In Figs. 10 (a) and (b), we examine the energy dependence of our predictions for two different intervals of mass Q. For Q_T not too small, we observe that A_{LL} in massive lepton pair production is well described by a scaling function of $x_T = 2Q_T/\sqrt{S}$, $A_{LL}(\sqrt{S}, Q_T) \simeq h_{\gamma^*}(x_T)$. In our discussion of the spin-averaged cross sections, we took $Ed^3\sigma/dp^3 = 10^{-3}\text{pb/GeV}^2$ as the minimum accessible cross. Combining the results in Fig. 5 with those in Fig. 10, we see that longitudinal asymmetries $A_{LL} = 20\%$, 7.5%, and 3% are predicted at this level of cross section at $\sqrt{S} = 50$, 200, and 500 GeV when $2 < Q < 3$ GeV, and $A_{LL} = 11\%$, 5%, and 2% when $5 < Q < 6$ GeV. For a given value of Q_T, smaller values of $\sqrt{S}$ result in greater asymmetries because $\Delta G(x)/G(x)$ grows with x.

The predicted cross sections in Fig. 5 and the predicted asymmetries in Fig. 10 should make it possible to optimize the choice of center-of-mass energy at which measurements might be carried out. At $\sqrt{S} = 500$ GeV, asymmetries are not appreciable in the interval of Q_T in which event rates are appreciable. At the other extreme, the choice of $\sqrt{S} = 50$ GeV does not allow a sufficient range in Q_T. Accelerator physics considerations favor higher energies since the instantaneous luminosity increases with $\sqrt{S}$. Investigations in the energy interval $\sqrt{S} = 150$ to 200 GeV would seem preferred.

In Fig. 11, we display predictions for A_{LL} in prompt real photon production for three values of the center-of-mass energy. These calculations are done at next-to-leading order in QCD. Dominance of the qg contribution is again evident as long as A_{LL} is not too small. So long as $Q_T \geq Q$, we note that the asymmetry in massive lepton-pair production is about the same size as that in prompt real photon production, as might be expected from the strong similarity of the production dynamics in the two cases. As in massive lepton-pair production, A_{LL} in prompt photon production is well described by a scaling function of $x_T = 2p_T/\sqrt{S}$, $A_{LL}(\sqrt{S}, p_T) \simeq h_\gamma(x_T)$. For $Ed^3\sigma/dp^3 = 10^{-3}\text{pb/GeV}^2$, we predict longitudinal asymmetries $A_{LL} = 31\%$, 17%, and 10% in real prompt photon production at $\sqrt{S} = 50$, 200, and 500 GeV.

V. DISCUSSION AND CONCLUSIONS

In this paper we focus on the Q_T distribution for $p+p \to \gamma^* + X$. We present and discuss calculations carried out in QCD at RHIC collider energies. We show that the differential cross section in the region $Q_T \geq Q/2$ is dominated by subprocesses initiated by incident gluons. Dominance of the qg contribution in the massive lepton-pair case is as strong as in the prompt photon case, $p + p \to \gamma + X$. As our calculations demonstrate, the Q_T distribution of massive lepton pair production offers a valuable additional method for direct measurement of the gluon momentum distribution. The method is similar in principle to the approach based on prompt photon production, but it avoids the experimental and theoretical

complications of photon isolation that beset studies of prompt photon production.

As long Q_T is large, the perturbative requirement of small $\alpha_s(Q_T)$ can be satisfied without a large value of Q. We therefore explore and advocate the potential advantages of studies of $d^2\sigma/dQdQ_T$ as a function of Q_T for modest values of Q, $Q \sim 2$ GeV, below the traditional Drell-Yan region.

For the goals we have in mind, it would appear best to restrict attention to the region in Q_T above the value at which the resummed result falls below the fixed-order perturbative expectation. A rough rule-of-thumb based on our calculations is $Q_T \geq Q/2$. Uncertainties associated with resummation make it impossible to use data on the Q_T distribution at small Q_T to extract precise information on parton densities.

In this paper we also present a calculation of the longitudinal spin-dependence of massive lepton-pair production at large values of transverse momentum. We provide polarization asymmetries as functions of transverse momenta that may be useful for estimating the feasibility of measurements of spin-dependent cross sections in future experiments at RHIC collider energies. The Compton subprocess dominates the dynamics in longitudinally polarized proton-proton reactions as long as the polarized gluon density $\Delta G(x, \mu_f)$ is not too small. As a result, two-spin measurements of inclusive prompt photon production in polarized pp scattering should constrain the size, *sign*, and Bjorken x dependence of $\Delta G(x, \mu_f)$. Significant values of A_{LL} (i.e., greater than 5 %) may be expected for $x_T = 2Q_T/\sqrt{S} > 0.10$ if the polarized gluon density $\Delta G(x, \mu_f)$ is as large as that in the GSA set of polarized parton densities. If so, the data could be used to determine the polarization of the gluon density in the nucleon. On the other hand, for small $\Delta G(x, \mu_f)$, dominance of the qg subprocess is lost, and $\Delta G(x, \mu_f)$ is inaccessible.

ACKNOWLEDGMENTS

Work in the High Energy Physics Division at Argonne National Laboratory is supported by the U.S. Department of Energy, Division of High Energy Physics, Contract W-31-109-

ENG-38. This work was supported in part by DOE contract DE-AC05-84ER40150 under which Southeastern Universities Research Association operates the Thomas Jefferson National Accelerator Facility.

REFERENCES

[1] S. Drell and T. M. Yan, Phys. Rev. Lett. **25**, 316 (1970); Ann. Phys. (NY) **66**, 578 (1971).

[2] E. L. Berger and J.-W. Qiu, Phys. Lett. **B248**, 371 (1990) and Phys. Rev. **D44**, 2002 (1991).

[3] H. Baer, J. Ohnemus, and J. F. Owens, Phys. Rev. **D42**, 61 (1990).

[4] P. Aurenche *et al*, Nucl. Phys. **B399**, 34 (1993).

[5] L. E. Gordon and W. Vogelsang, Phys. Rev. **D48**, 3136 (1993) and **D50**, 1901 (1994); M. Glück, L. E. Gordon, E. Reya, and W. Vogelsang, Phys. Rev. Lett. **73**, 388 (1994); L. E. Gordon, Nucl. Phys. **B501**, 175 (1997).

[6] E. L. Berger, L. E. Gordon, and M. Klasen, Phys. Rev. **D58**, 074012 (1998) and hep-ph/9906402.

[7] E. L. Berger, X.-F. Guo, and J.-W. Qiu, Phys. Rev. Lett. **76**, 2234 (1996); Phys. Rev. **D54**, 5470 (1996). E. L. Berger, X.-F. Guo, and J.-W. Qiu, in *'97 QCD and High Energy Hadronic Interactions*, Proceedings of the XXXIInd Rencontres de Moriond, Les Arcs, France, March, 1997, edited by J. Tran Thanh Van (Editions Frontieres, Paris, 1997) pp 267 - 274.

[8] P. B. Arnold and M. H. Reno, Nucl. Phys. **B319**, 37 (1989), and erratum Nucl. Phys. **B330**, 284 (1990); R. J. Gonsalves, J. Pawlowski, and C.-F. Wai, Phys. Rev. **D40**, 2245 (1989).

[9] J. Collins, D. Soper, and G. Sterman, Nucl. Phys. **B250**, 199 (1985); J. Collins and D. Soper, Nucl. Phys. **B193**, 381 (1981), Nucl. Phys. **B197**, 446 (1982), and erratum Nucl. Phys. **B213**, 545 (1983).

[10] C. Davies, B. Webber, and W. J. Stirling, Nucl. Phys. **B256**, 413 (1985); C. Davies and

W. J. Stirling, Nucl. Phys. **B244**, 337 (1984).

[11] G. Altarelli, R. K. Ellis, M. Greco, and G. Martinelli, Nucl. Phys. **B246**, 12 (1984). For a recent treatment and list of references, see R. K. Ellis, D. A. Ross, and S. Veseli, Nucl. Phys. **B503**, 309 (1997).

[12] P. B. Arnold and R. Kauffman, Nucl. Phys. **B349**, 381 (1991).

[13] G. A. Ladinsky and C. P. Yuan, Phys. Rev. **D50**, 4239 (1994).

[14] E. L. Berger and D. E. Soper, Nucl. Phys. **B247**, 29 (1984).

[15] S. Chang, C. Coriano, R. D. Field, and L. E. Gordon, Nucl. Phys. **B512** 393, (1998); S. Chang, C. Coriano, and R. D. Field, Nucl. Phys. **B528** 285, (1998).

[16] S. Frixione and W. Vogelsang, hep-ph/9908387.

[17] A. D. Martin, R. G. Roberts, W. J. Stirling, and R. S. Thorne, Eur. Phys. J. **C4**, 463 (1998).

[18] T. Gehrmann and W. J. Stirling, Phys. Rev. **D53**, 6100 (1996).

[19] E. L. Berger and L. E. Gordon, Phys. Rev. **D58**, 114024 (1998).

FIGURES

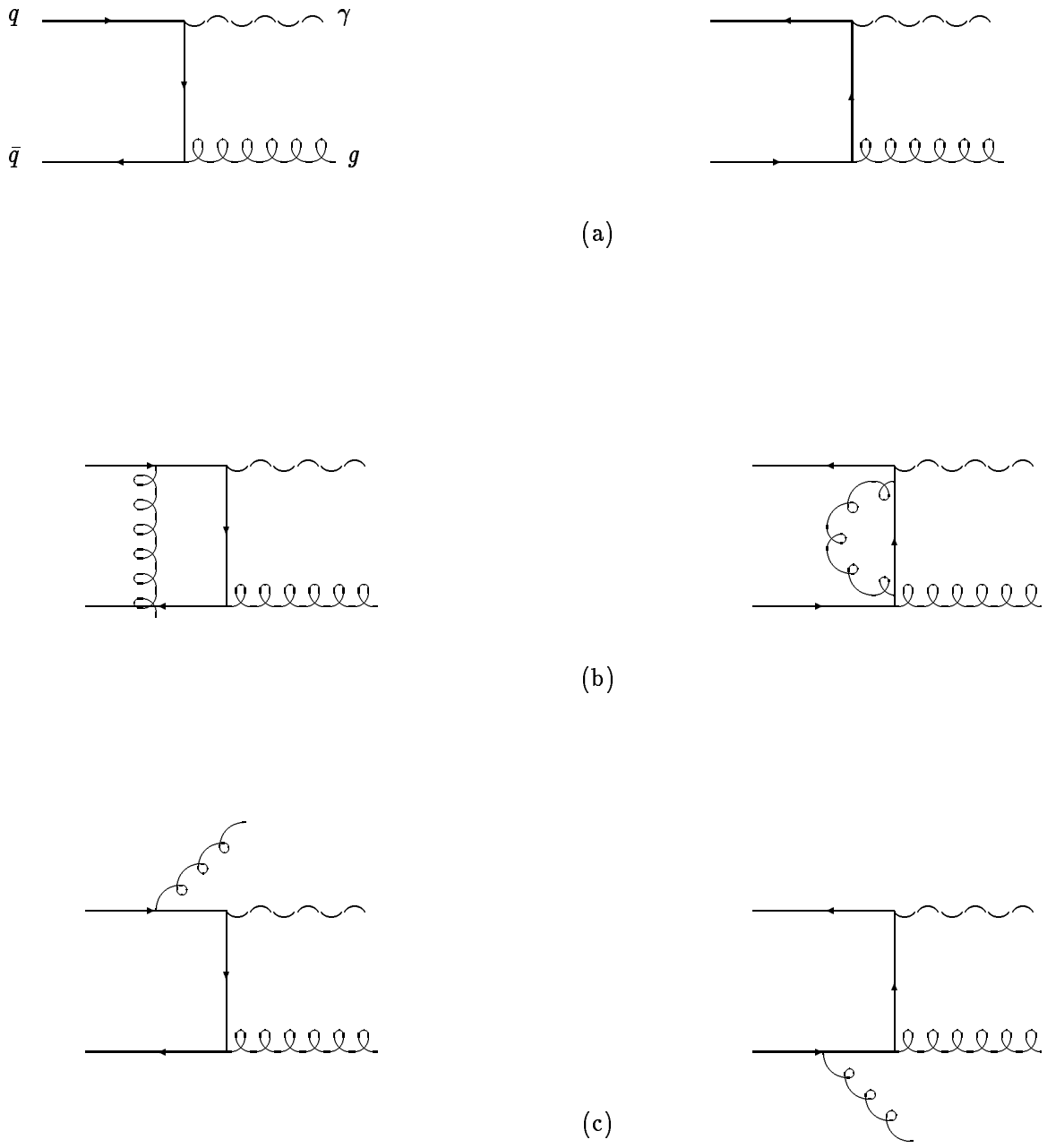

FIG. 1. (a)Lowest-order Feynman diagrams for the direct process $q+\bar{q} \rightarrow \gamma+g$. (b) Examples of virtual gluon loop diagrams. (c) Examples of next-to-leading order three-body final-state diagrams.

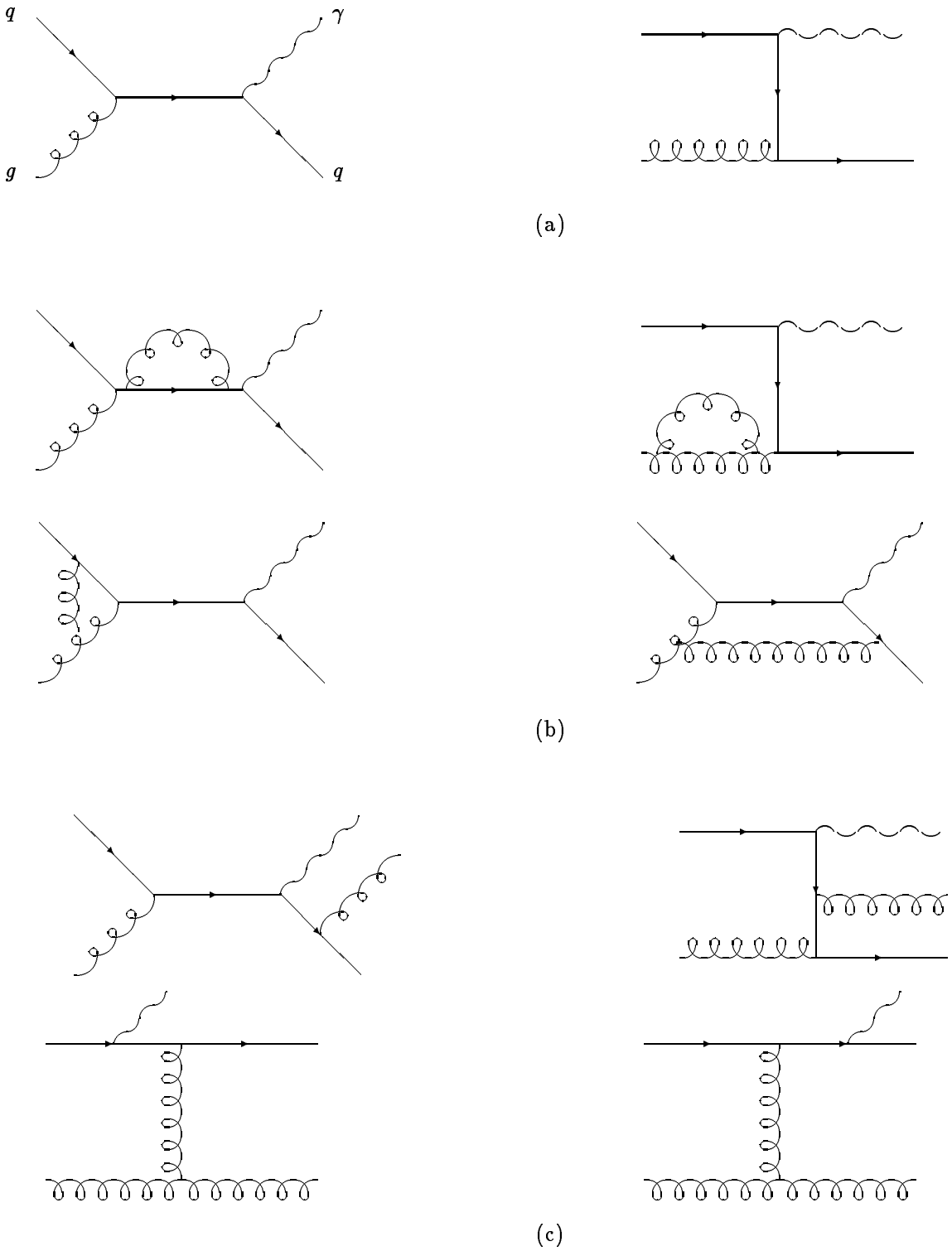

FIG. 2. As in Fig. 1, but for the subprocesses initiated by the $q + g$ initial state.

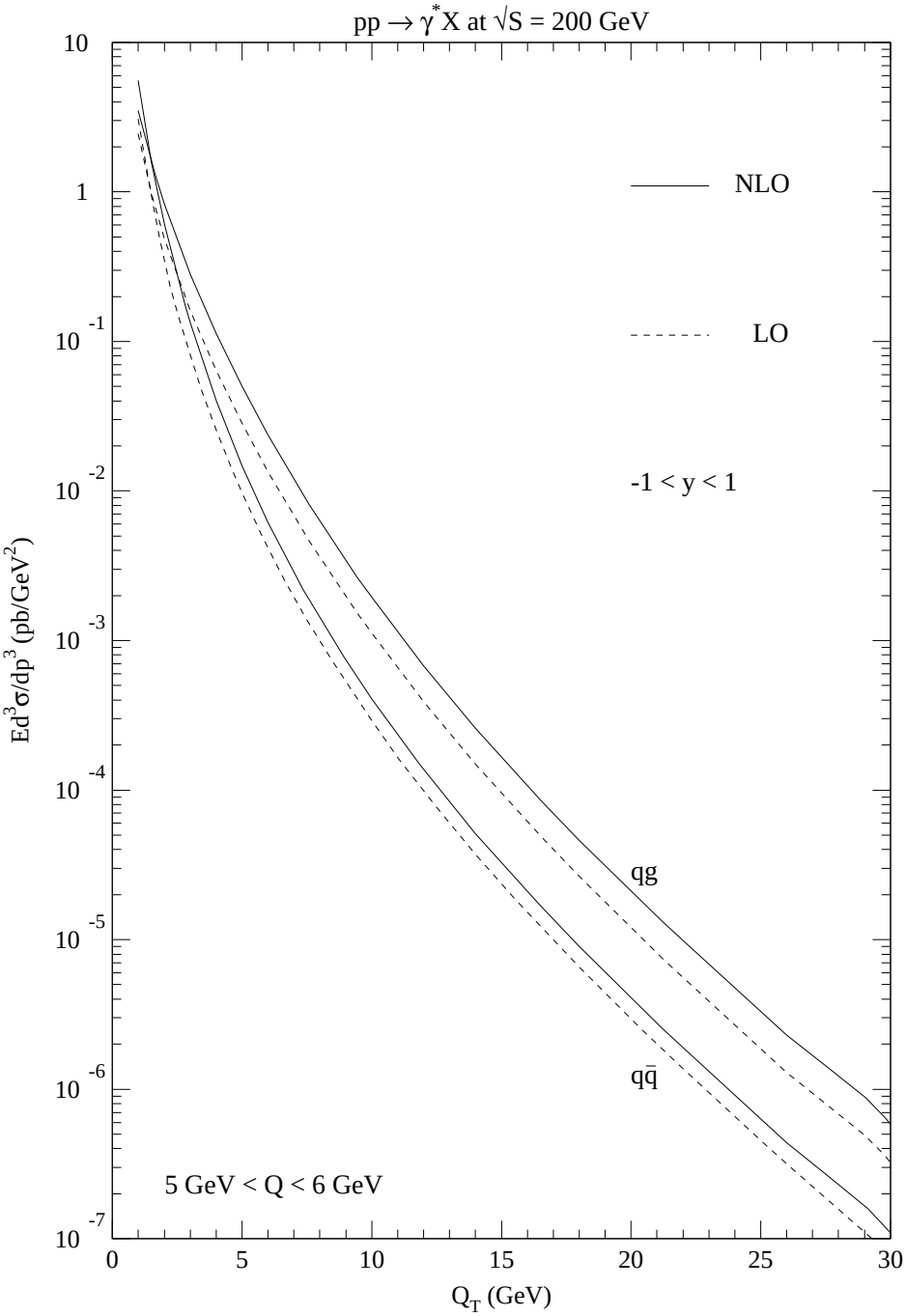

FIG. 3. Lowest order (dashed lines) and next-to-leading order (solid lines) perturbative calculations of the invariant inclusive cross section $Ed^3\sigma/dp^3$ as a function of Q_T for $pp \to \gamma^* X$ at $\sqrt{S} =$ 200 GeV, in the $\overline{\rm MS}$ scheme. Contributions from the qg and $q\bar{q}$ channels are shown separately. The results are averaged over the rapidity interval - $1.0 < y < 1.0$ and over the interval $5.0 < Q < 6.0$ GeV.

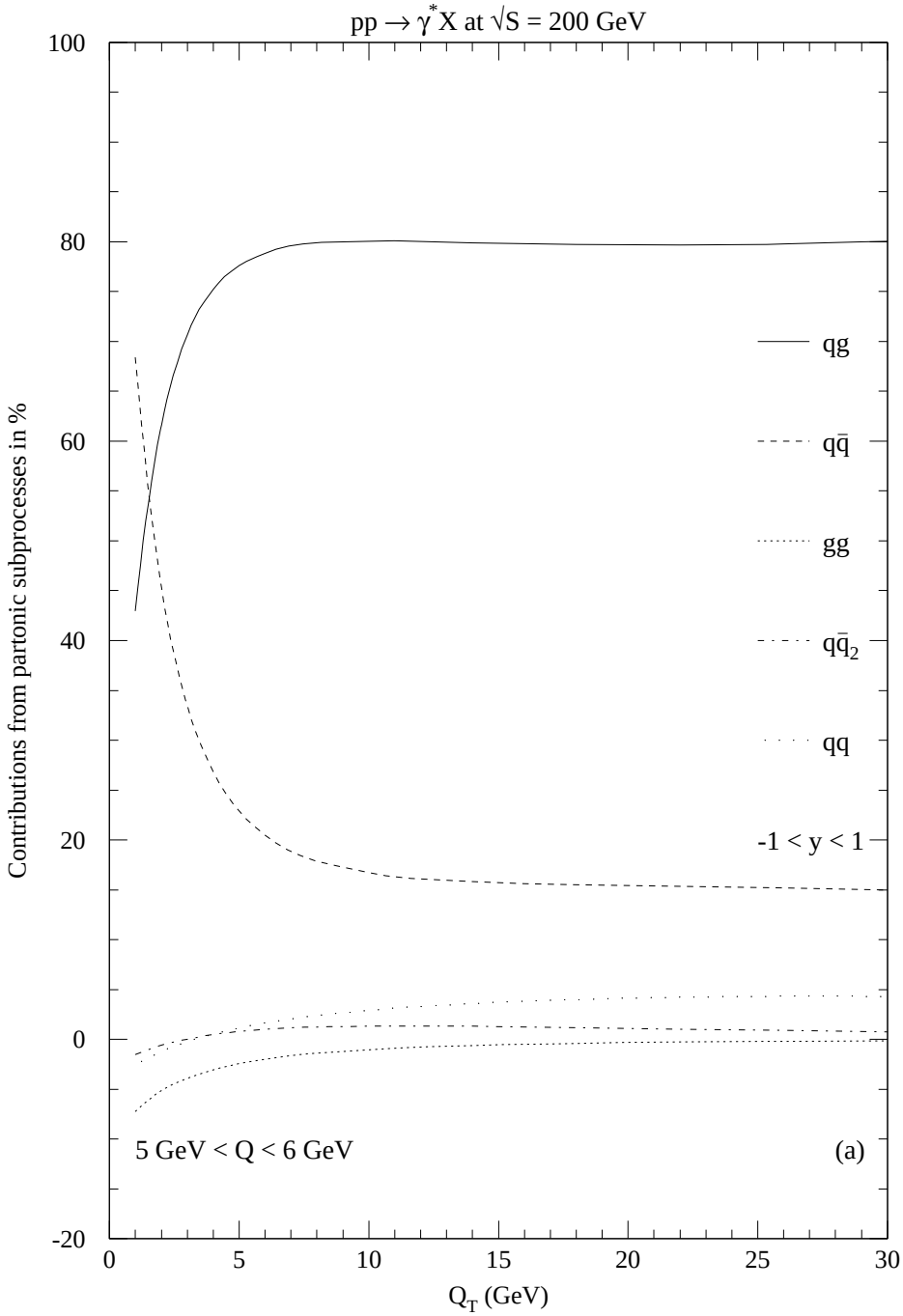
pp → γ* X at √S = 200 GeV
Contributions from partonic subprocesses in %
100
80
60
40
20
0
-20
0
5
10
15
20
25
30
Q_T (GeV)
qg
qq̄
gg
qq̄2
qq
-1 < y < 1
5 GeV < Q < 6 GeV
(a)

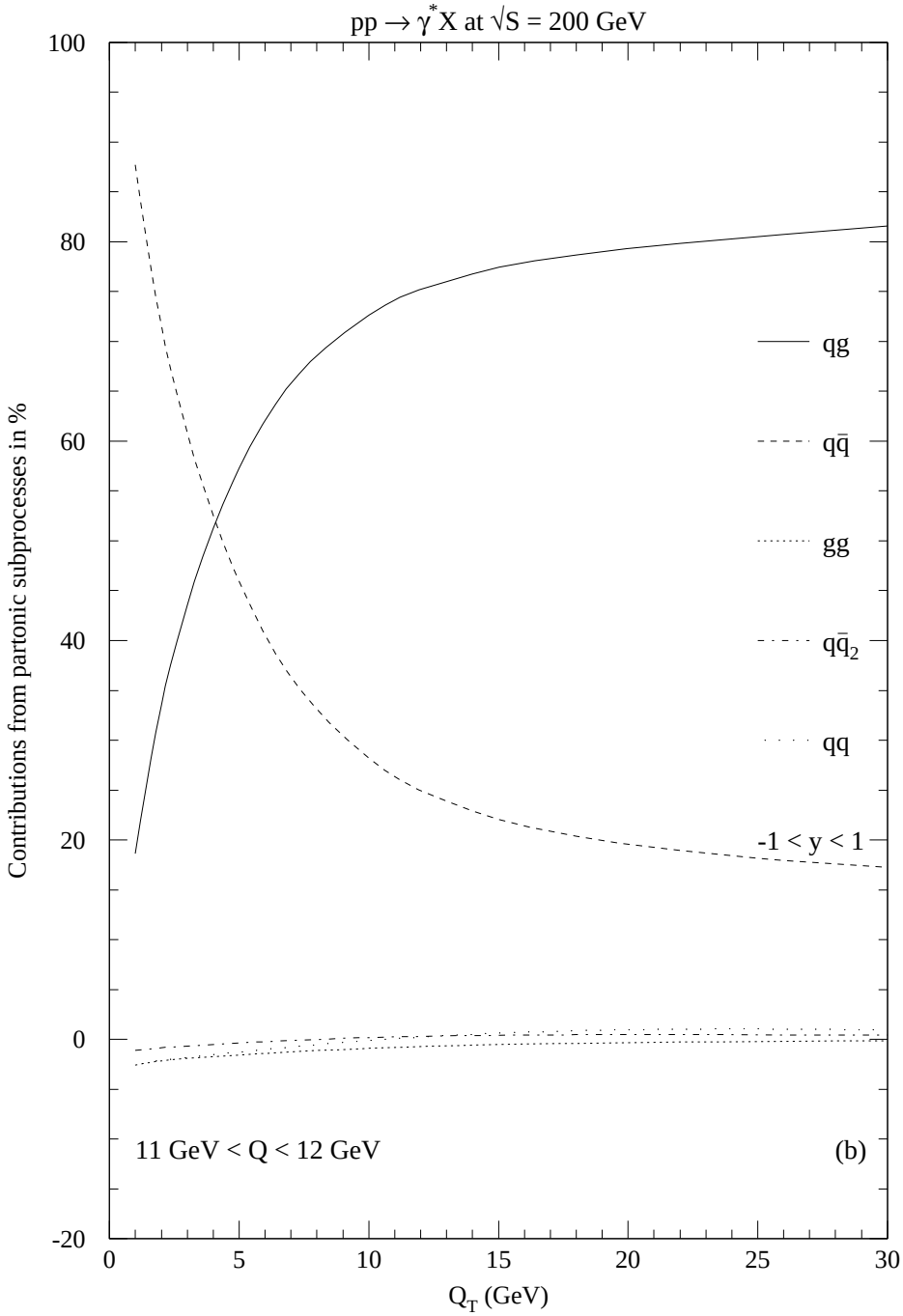
pp → γ* X at √S = 200 GeV
Contributions from partonic subprocesses in %
100
80
60
40
20
0
-20
0
5
10
15
20
25
30
Q_T (GeV)
qg
qq̄
gg
qq̄2
qq
-1 < y < 1
11 GeV < Q < 12 GeV
(b)

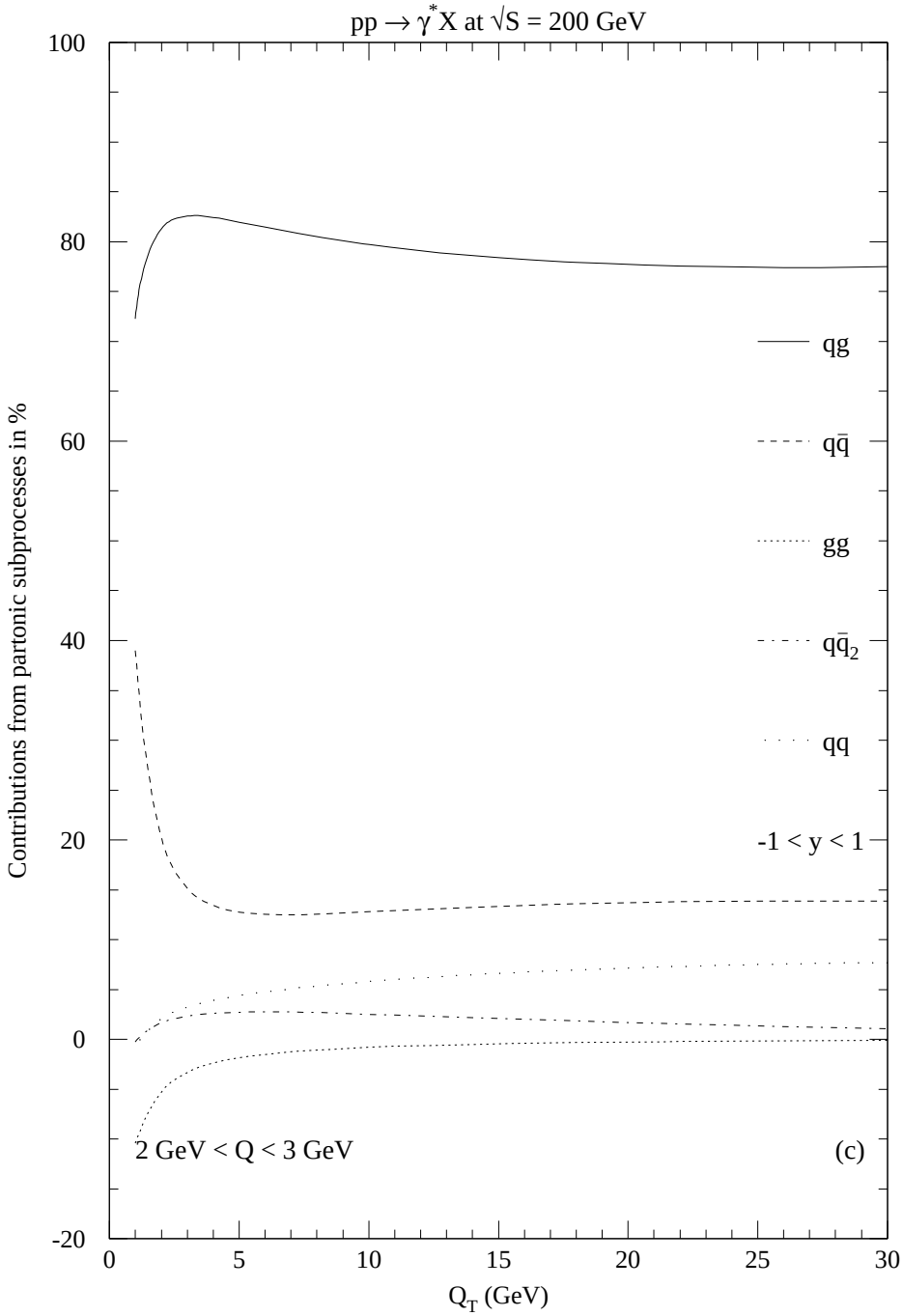

FIG. 4. Contributions from the various partonic subprocesses to the invariant inclusive cross section $Ed^3\sigma/dp^3$ as a function of Q_T for $pp \to \gamma^* X$ at $\sqrt{S} = 200$ GeV. The cross section is averaged over the rapidity interval -1.0 $< y <$ 1.0 and over the intervals (a) 5.0 $< Q <$ 6.0 GeV, (b) 11.0 $< Q <$ 12.0 GeV, and (c) 2.0 $< Q <$ 3.0 GeV. The contributions are labeled by qg (solid), $q\bar{q}$ (dashed), gg (dotted), $q\bar{q}_2$ non-factorizable parts (dot-dashed), and qq (wide dots).

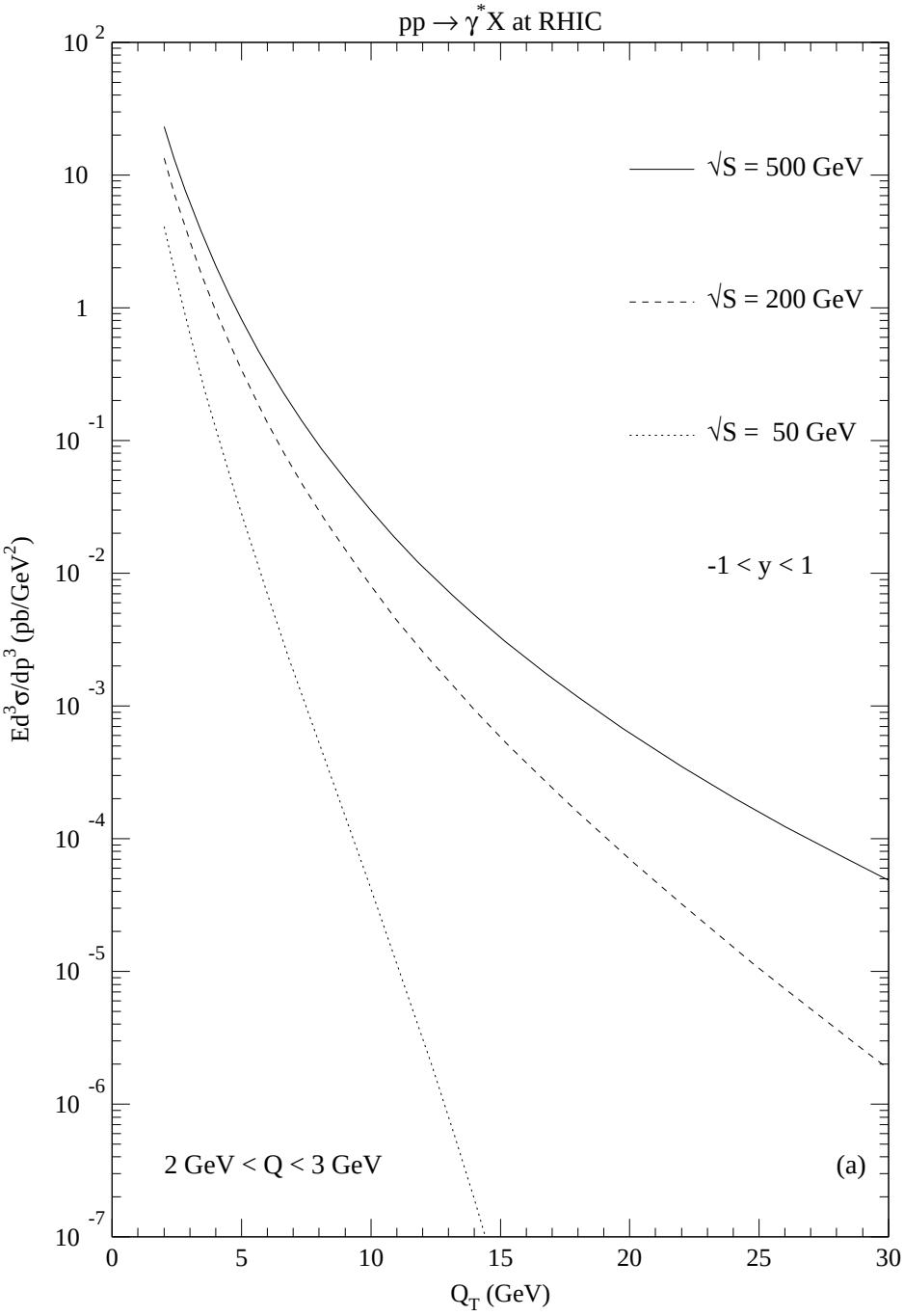
pp → γ* X at RHIC
√S = 500 GeV
√S = 200 GeV
√S = 50 GeV
-1 < y < 1
2 GeV < Q < 3 GeV
(a)
Ed³σ/dp³ (pb/GeV²)
Q_T (GeV)
10 2
10
1
10 -1
10 -2
10 -3
10 -4
10 -5
10 -6
10 -7
0
5
10
15
20
25
30

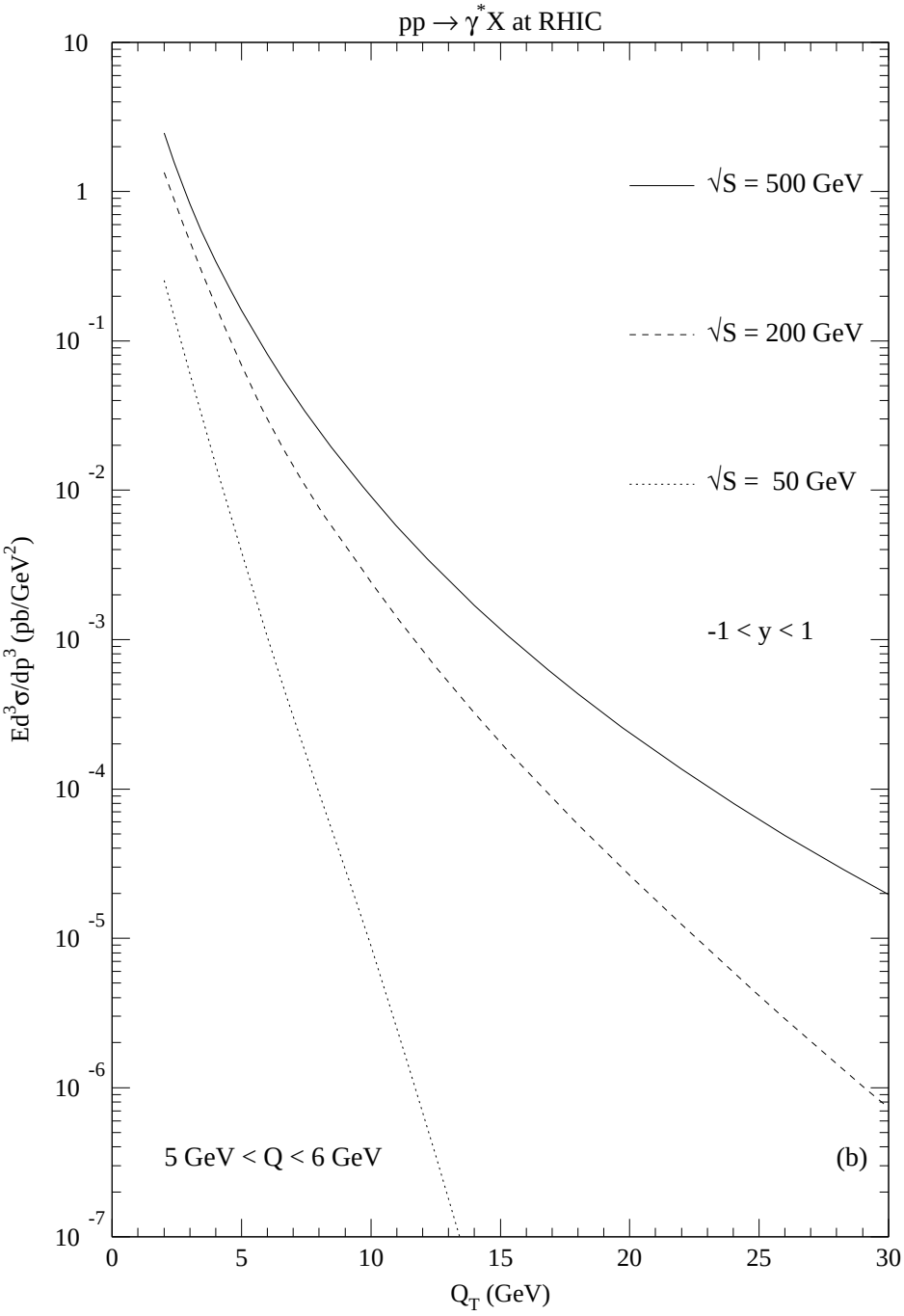

FIG. 5. Differential cross sections $Ed^3\sigma/dp^3$ as a function of Q_T for for $pp \to \gamma^* + X$ at $\sqrt{S} =$ 50, 200, and 500 GeV, averaged over the rapidity interval -1.0 $< y <$ 1.0 and the mass intervals (a) 2.0 $< Q <$ 3.0 GeV, and (b) 5.0 $< Q <$ 6.0 GeV.

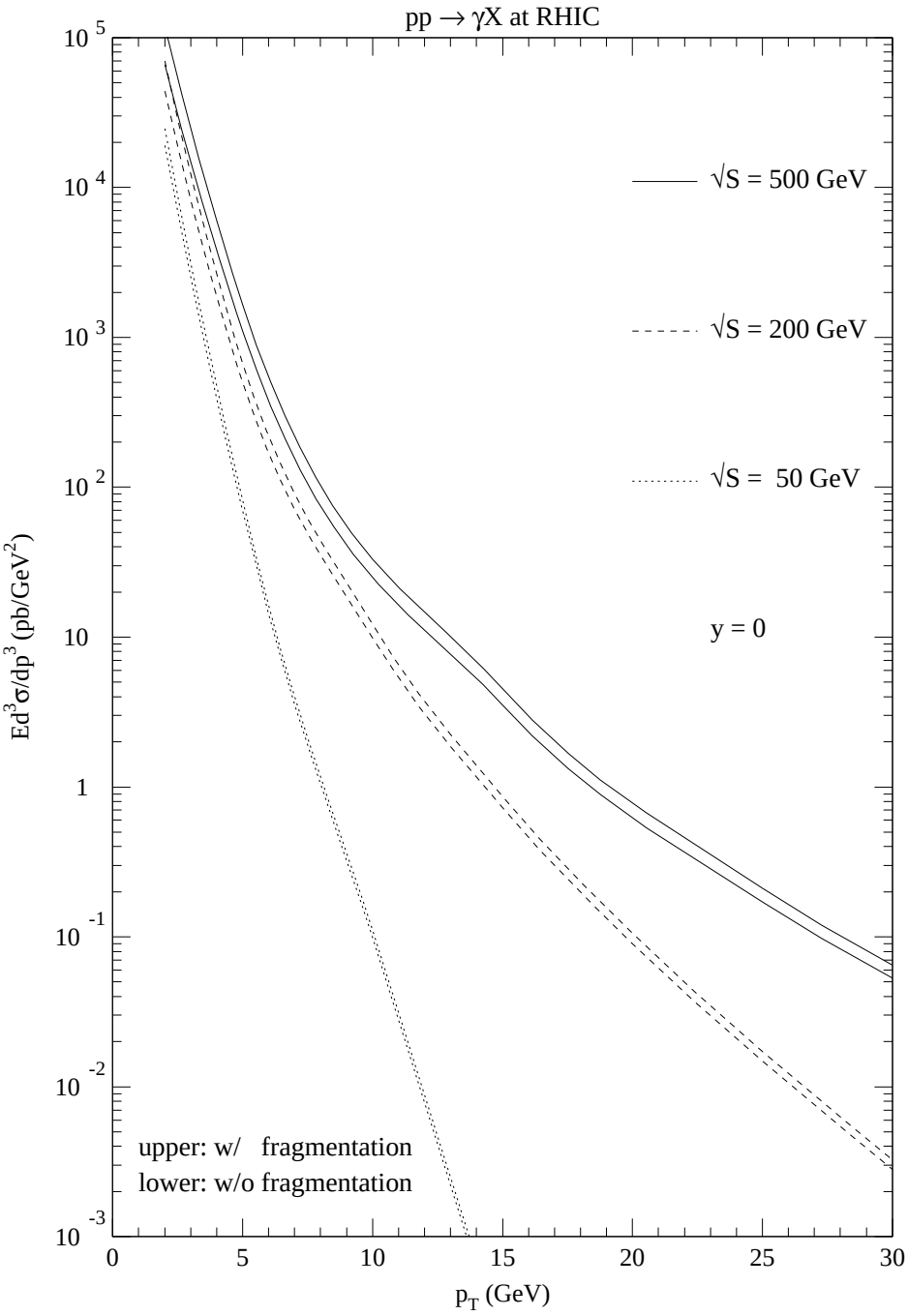

FIG. 6. Differential cross sections $Ed^3\sigma/dp^3$ at rapidity $y = 0$ as a function of p_T for real photon production $pp \to \gamma X$ at $\sqrt{S} = 50$, 200, and 500 GeV for two cases: no fragmentation terms included (lower) and the inclusive case with full fragmentation included (upper).

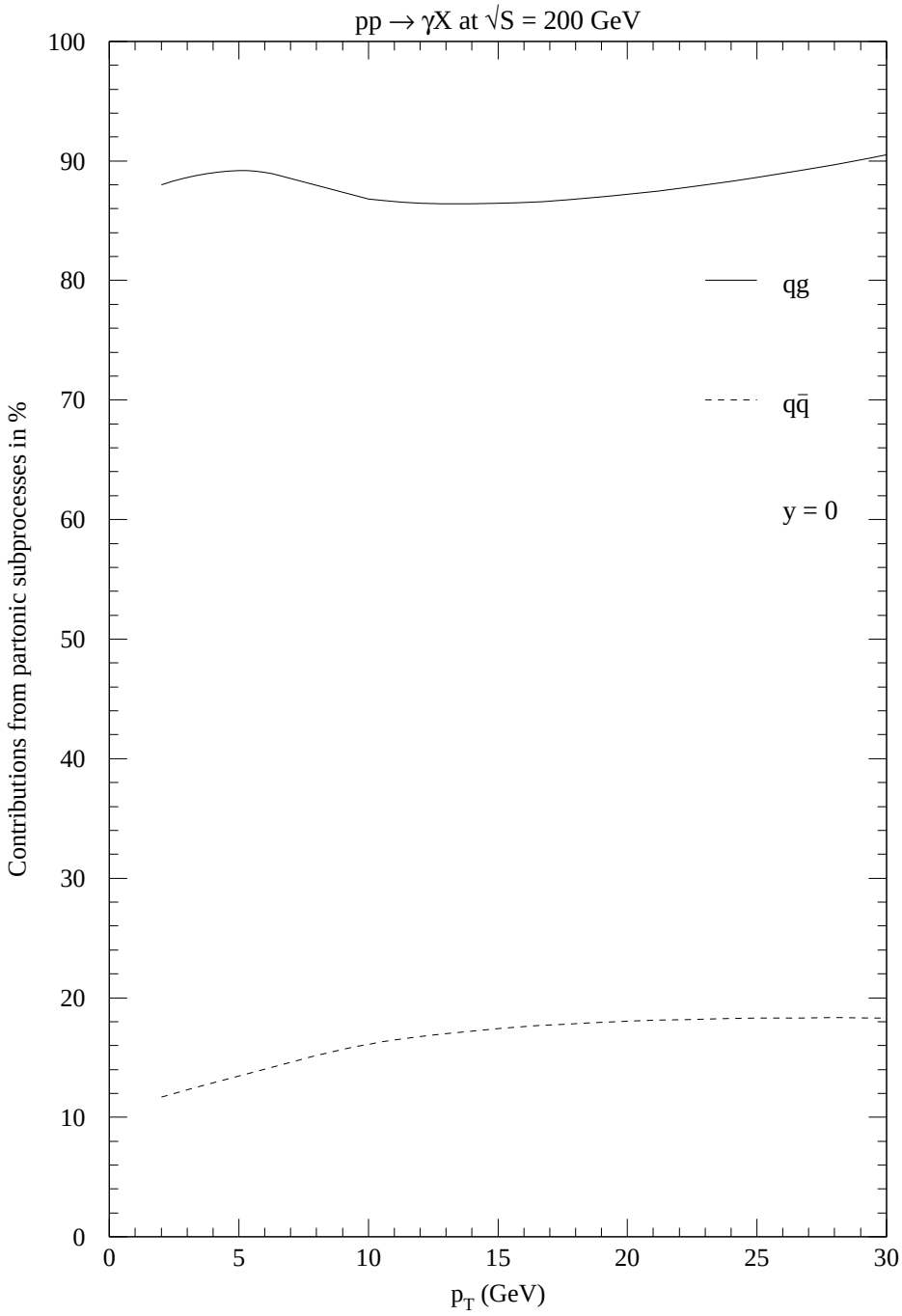

FIG. 7. Fractional contributions from the next-to-leading order $q\bar{q}$ and the qg channels to the differential cross sections $Ed^3\sigma/dp^3$ as a function of p_T for real photon production $pp \to \gamma X$ at $\sqrt{S} = 200$ GeV and rapidity $y = 0$. No fragmentation terms are included.

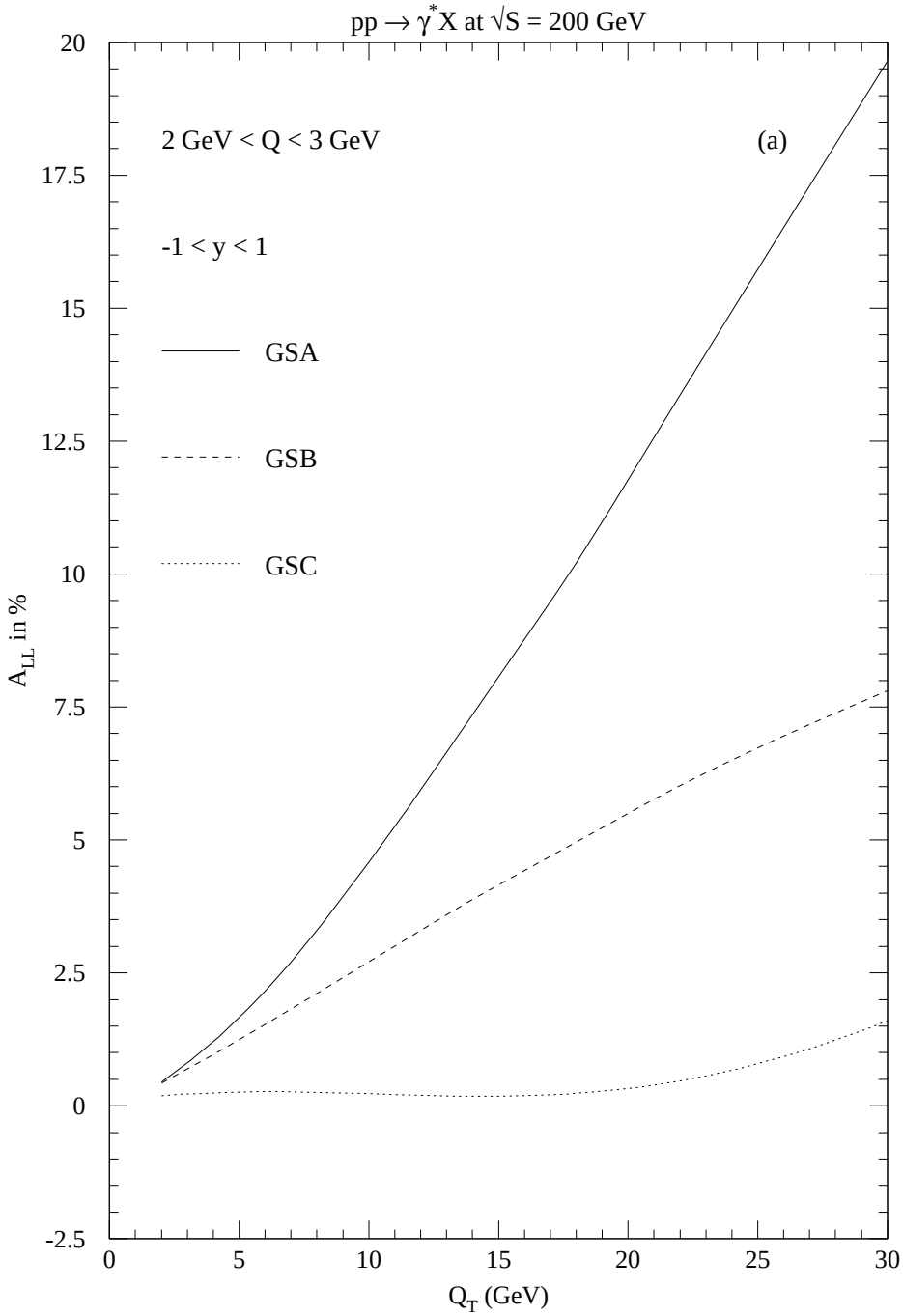
pp → γ* X at √S = 200 GeV
2 GeV < Q < 3 GeV
(a)
-1 < y < 1
GSA
GSB
GSC
A_LL in %
Q_T (GeV)
20
17.5
15
12.5
10
7.5
5
2.5
0
-2.5
0
5
10
15
20
25
30

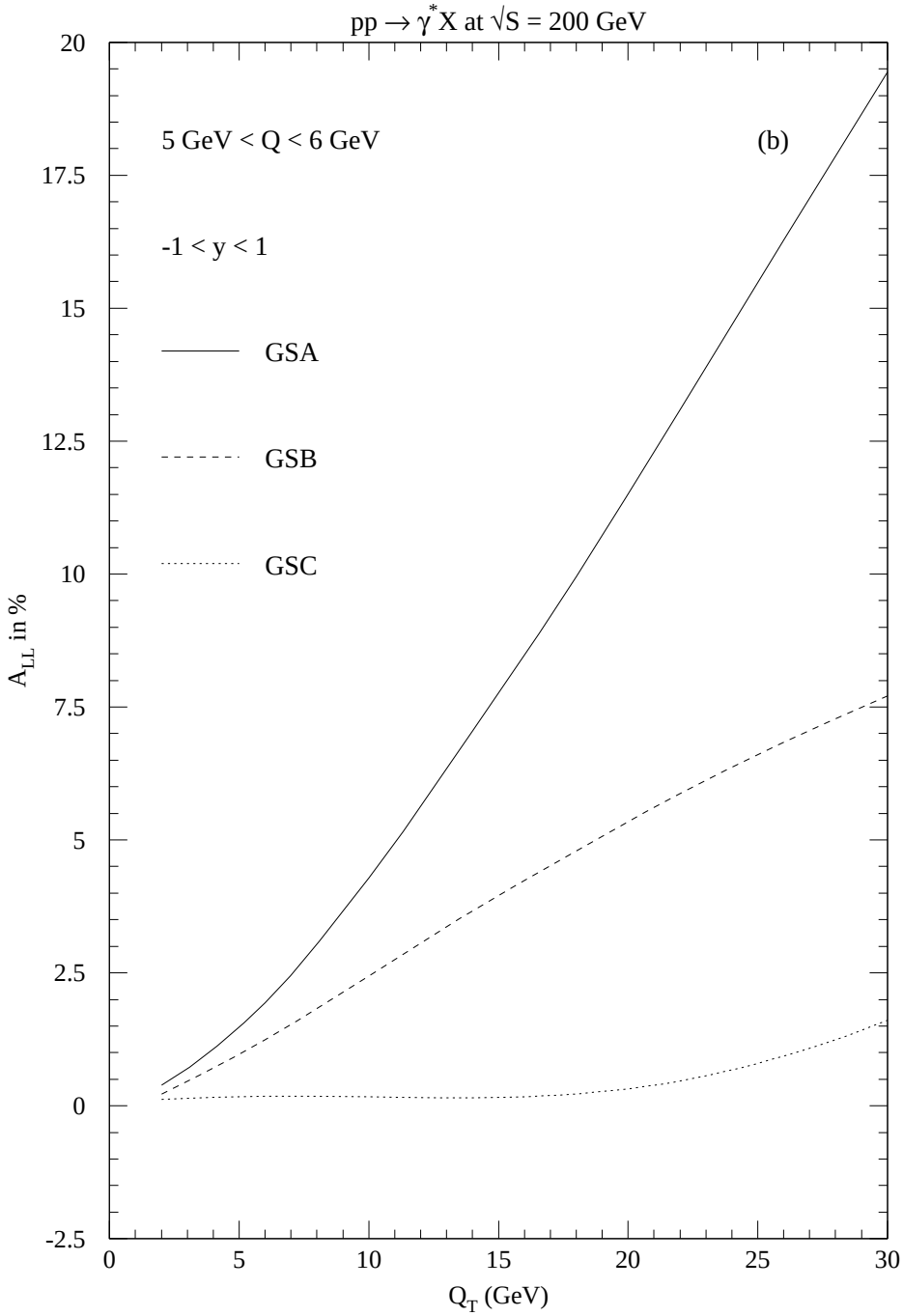
pp → γ* X at √S = 200 GeV
5 GeV < Q < 6 GeV
(b)
-1 < y < 1
GSA
GSB
GSC
A_LL in %
Q_T (GeV)
20
17.5
15
12.5
10
7.5
5
2.5
0
-2.5
0
5
10
15
20
25
30

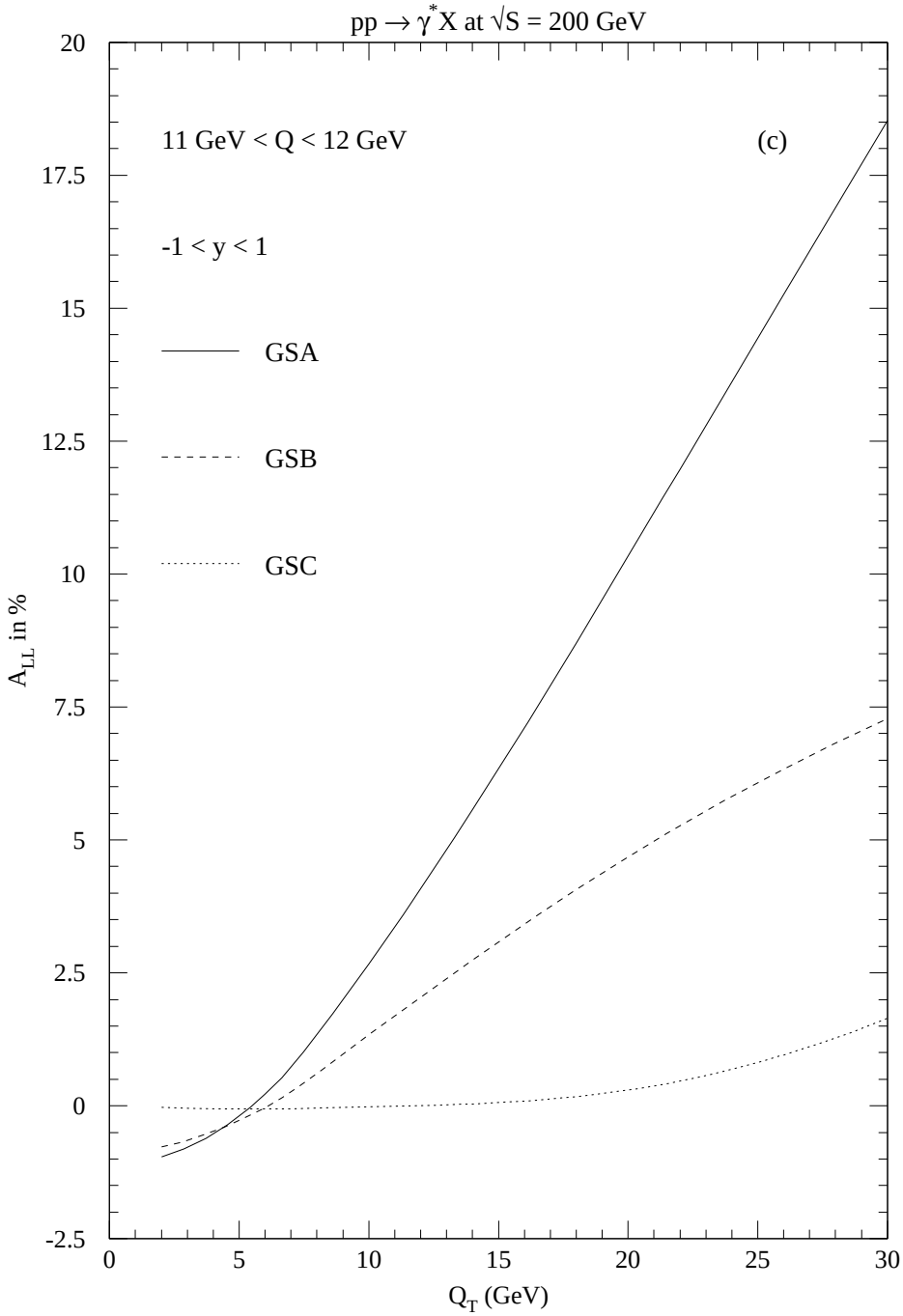

FIG. 8. Computed longitudinal asymmetry A_{LL} as a function of Q_T for $pp \to \gamma^* X$ at $\sqrt{S} = 200$ GeV. The asymmetry is averaged over the rapidity interval -1.0 $< y <$ 1.0 and over the intervals (a) 2.0 $< Q <$ 3.0 GeV, (b) 5.0 $< Q <$ 6.0 GeV, and (c) 11.0 $< Q <$ 12.0 GeV, for three choices of the polarized parton densities, GSA, GSB, and GSC.

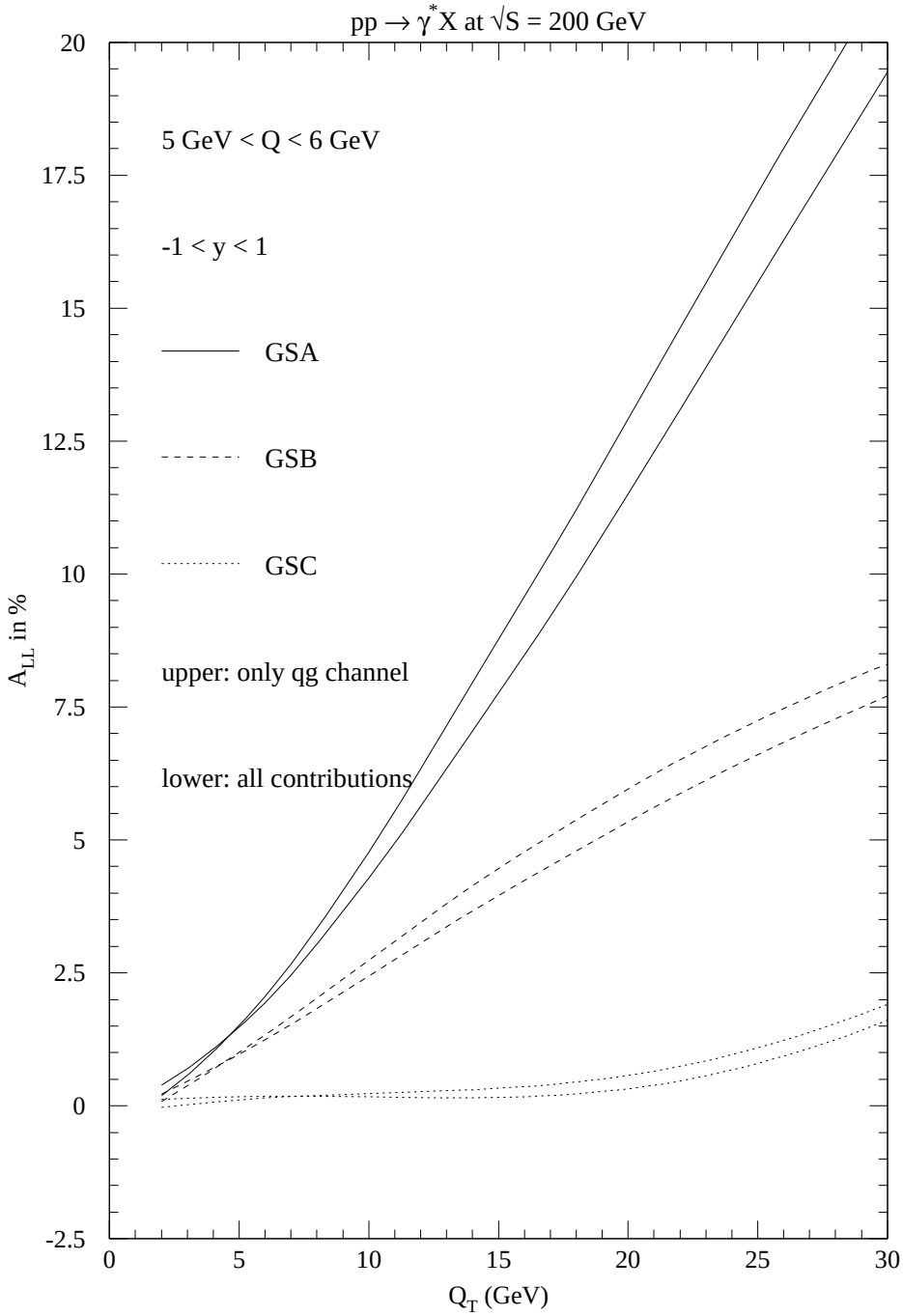

FIG. 9. Comparison of the contribution of the qg subprocess (upper curve) to the longitudinal asymmetry A_{LL} with the total (lower curve) as a function of Q_T for $pp \to \gamma^* X$ at $\sqrt{S} = 200$ GeV. The asymmetry is averaged over the rapidity interval -1.0 $< y <$ 1.0 and over the interval 5.0 $< Q <$ 6.0 GeV. Results are shown for three sets of spin-dependent parton densities.

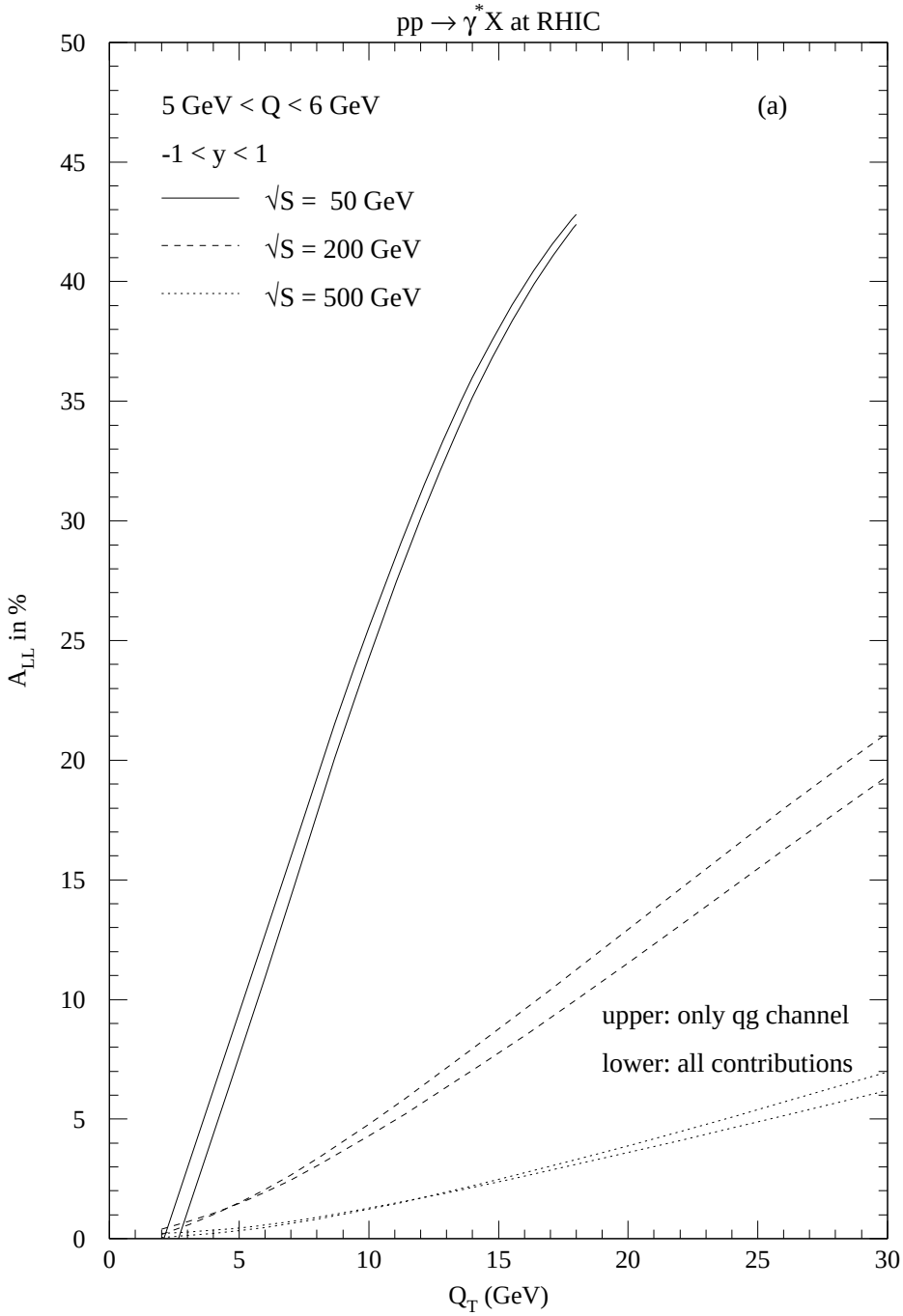
pp → γ* X at RHIC
5 GeV < Q < 6 GeV
(a)
-1 < y < 1
√S = 50 GeV
√S = 200 GeV
√S = 500 GeV
upper: only qg channel
lower: all contributions
A_LL in %
Q_T (GeV)
0
5
10
15
20
25
30
35
40
45
50

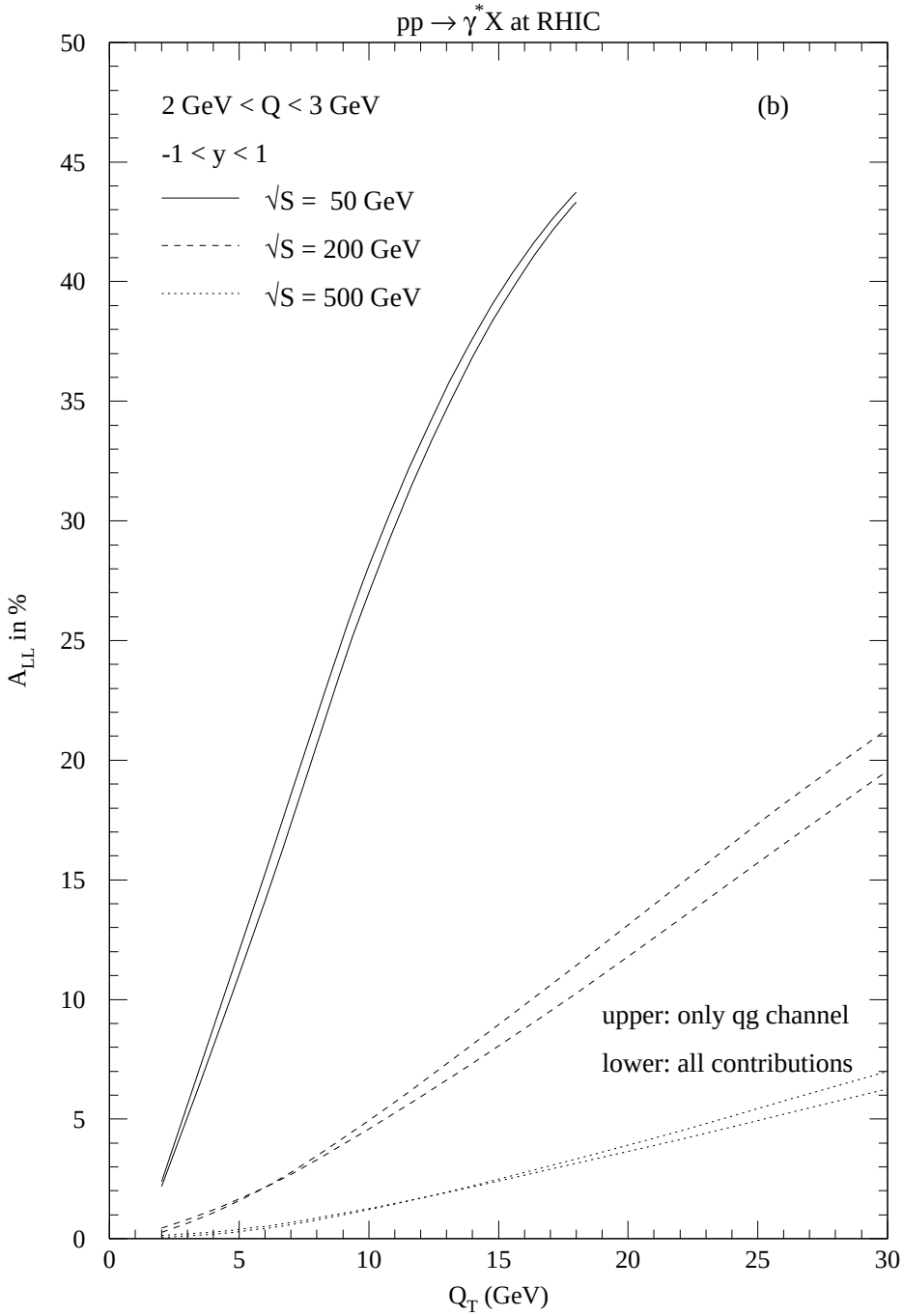

FIG. 10. Computed longitudinal asymmetry A_{LL} as a function of Q_T for for $pp \to \gamma^* + X$ at $\sqrt{S}$ = 50, 200, and 500 GeV, averaged over the rapidity interval -1.0 < y < 1.0 and the mass intervals (a) 5.0 < Q < 6.0 GeV and (b) 2.0 < Q < 3.0 GeV. Shown are both the complete answer at leading-order and the contribution from the qg subprocess. The GSA set of polarized parton densities is used.

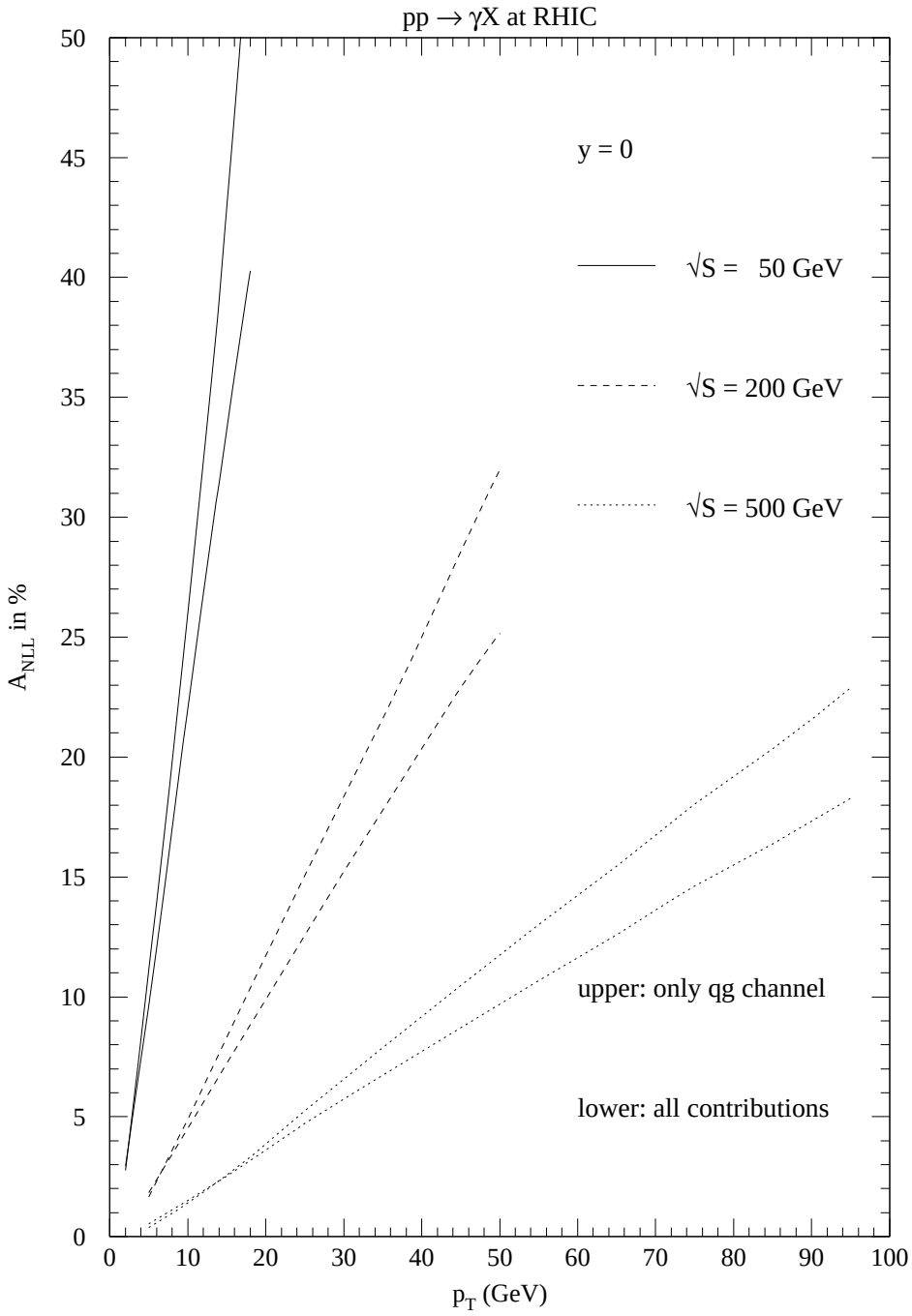

FIG. 11. Computed longitudinal asymmetry A_{LL} as a function of p_T for real photon production $pp \to \gamma + X$ at $\sqrt{S} = 50$, 200, and 500 GeV and rapidity $y = 0$. Shown are both the complete answer at leading-order and the contribution from the qg subprocess. The GSA set of polarized parton densities is used.